Clays and Clay Minerals, Vol. 64, No. 4, 488–502, 2016.

INTERCALATION OF ETHYLENE GLYCOL IN SMECTITES: SEVERAL MOLECULAR SIMULATION MODELS VERIFIED BY X-RAY DIFFRACTION DATA

MAREK SZCZERBA[1,*] AND ANDREY G. KALINICHEV[2]

[1] Institute of Geological Sciences, Polish Academy of Sciences, Kraków, Poland
[2] Laboratoire SUBATECH (UMR 6457), Ecole des Mines de Nantes, Nantes, France

Abstract—Organo-clays represent a special challenge for molecular simulations because they require accurate representation of the clay and the organic/aqueous sections of the model system and accurate representation of the interactions between them. Due to the broad range of force-field models available, an important question to ask is which sets of parameters will best suit the molecular modeling of the organo-intercalated smectites? To answer this question, the structure of the ethylene glycol (EG)-smectite complex is used here as a testing model because the intercalation of EG in smectites provides a stable interlayer complex with relatively constant basal spacing.

Three smectite samples with substantially different layer charge and charge localization were selected for X-ray diffraction (XRD) measurements. Their molecular models were built and molecular-dynamics simulations performed using various combinations of the organic force fields (*CGenFF*, *GAFF*, *CVFF*, and *OPLS-aa*) with *ClayFF* and *INTERFACE* force fields used to describe smectites. The simulations covered a range of different EG and water contents. For every structure, the density distribution of interlayer species along the direction perpendicular to the layer plane was calculated and then used to optimize the XRD patterns for these simulated models.

A comparison of these results with experimental XRD patterns shows very large discrepancies in the structures and basal spacings obtained for different layer charges as well as for different force fields and their combinations. The most significant factor affecting the accuracy of the calculated XRD patterns was the selection of the clay-mineral force-field parameters. The second important conclusion is that a slight modification of the basal oxygen parameters for non-electrostatic interactions (increase of their effective atomic diameters) may be a simple and straightforward way to improve significantly the agreement between the modeled XRD patterns with experiments, especially for high-charge smectites. Generally, among organic force fields, the least accurate results were obtained with *CGenFF*. For unmodified *ClayFF*, its combination with *GAFF* gave the best results, while the two other sets (*OPLS-aa* and *CVFF*) gave the best results in combination with *ClayFFmod*. The *INTERFACE* and *INTERFACEmod* produced much better results for low-charge montmorillonite than for high-charge smectites.

Key Words—Ethylene Glycol, Molecular Dynamics, Smectite, X-ray Diffraction.

INTRODUCTION

Recent growing interest in organo-clay nanocomposites is clearly reflected in the development of computational molecular modeling approaches to quantitative understanding of the structural and dynamic behavior of such systems (*e.g.* Zeng *et al.*, 2003; Suter and Coveney, 2009; Suter *et al.*, 2011, 2015; Greathouse *et al.*, 2014; Heinz and Ramezani-Dakhel, 2016). Apart from the atomistic structural data necessary to construct the molecular models, the most fundamental information required to perform such simulations is contained in the sets of parameters describing interatomic interactions in the systems modeled, often referred to collectively as the 'force fields.' Even though in the literature several widely used and well tested classical force fields are available for molecular modeling of clays and related inorganic materials (*e.g.* Heinz *et al.*, 2005), and an even larger number of force fields are available for molecular simulations of organic and bio-organic molecules (*e.g.* Guvench and MacKerell, 2008), molecular simulations often leave unanswered the important question of finding an optimal combination of the force-field parameters for accurate molecular modeling of both the organic and inorganic parts of the composite systems. Estimating the actual predictive capabilities of such simulations is certainly a non-trivial task. In order to address this issue quantitatively, a testing model is needed which should be known to provide a stable interlayer complex and should be supported by sufficient amounts of reliable experimental data for comparison with the simulated results. For these reasons, complexes of smectites with ethylene glycol (EG)-water mixtures were selected for the present study.

* E-mail address of corresponding author:
ndszczer@cyf-kr.edu.pl
DOI: 10.1346/CCMN.2016.0640411

This paper is published as part of a special issue on the subject of 'Computational Molecular Modeling.' Some of the papers were presented during the 2015 Clay Minerals Society-Euroclay Conference held in Edinburgh, UK.

Intercalation of EG in hydrated divalent ion-smectites is known to provide a structure with relatively constant basal spacing (*e.g.* Mosser-Ruck *et al.*, 2005). During this process, EG molecules penetrate into the interlayer spaces of the swelling clays, leading to the formation of a two-layer structure ($d \approx 17$ Å). For the purpose of interpreting XRD data, a simplified model of this complex was proposed by Reynolds (1965). Further studies have shown that the basal spacing is larger for clay minerals with lower layer charge, but that it also depends on the localization of the charge, the type of the exchangeable cations, the particle size, and the relative humidity (Harward and Brindley, 1965; Brindley, 1966; Harward *et al.*, 1969; Środoń, 1980; Sato *et al.*, 1992). If the charge is located in the tetrahedral sheet then the basal-spacing values are smaller than those observed when the charge is located in the octahedral sheet (Sato *et al.*, 1992). Other studies showed that smectites may form a one-layer EG complex instead of the two-layer complex at very low relative humidities (Eberl *et al.*, 1987), or with K^+ as the exchange cation even at intermediate humidities (Eberl *et al.*, 1986). The experimental observations were, to some extent, explained with the help of molecular simulations, *e.g.* the preference of formation of bilayer structures and the preferred number of water molecules in the structure for the Ca^{2+} form (Szczerba *et al.*, 2014). Several methods of clay glycolation with specific technical details are possible and Mosser-Ruck *et al.* (2005) demonstrated certain differences and inconsistencies between them. The formation of monolayer or bilayer complexes was found to be dependent on the type of interlayer cation and the concentration of EG in the close vicinity of the smectite (the 'glycolation protocol'). A gradual loss of EG from the complex with smectite also occurs because of the equilibration between the complex and the surrounding environment. X-ray measurements on such samples should, therefore, be performed relatively quickly (within a few hours) of glycolation. The dynamics of EG intercalation into smectites was studied by Svensson and Hansen (2010) using synchrotron XRD techniques; those authors showed that EG molecules replaced H_2O in the interlayer space, but still left significant amounts of water in the structure.

The present study was undertaken in order to investigate the effects of different combinations of force-field parameters on the accuracy of a two-EG layer structure representation. For this purpose, inorganic (clay) and organic (EG) force-field parameters needed to be coupled in a single simulation.

For clay minerals, several force-field parameterizations exist that have been used for molecular simulations of these structures over the past three decades. These parameters can be divided into two main groups: those that rely on the assumption of a rigid clay framework and those which allow partial or full flexibility of the structure. The parameterizations of the former kind were developed earlier (*e.g.* Skipper *et al.*, 1991; Smith, 1998); these are inherently limited, however, and can lead to incorrect representation of the processes of adsorption, surface hydration, hydrogen bonding, diffusion rates, *etc.* (*e.g.* Cygan *et al.*, 2009). The flexible force-field parameterizations are currently used much more widely (*e.g.* Hill and Sauer, 1995; Teppen *et al.*, 1997; Sato *et al.*, 2001; Manevitch and Rutledge, 2004; Cygan *et al.*, 2004; Heinz *et al.*, 2005). Only the parameterizations of Heinz *et al*. (2005) and *ClayFF* (Cygan *et al.*, 2004) have been shown to give cleavage energies that correspond reasonably well to the experimental values (Heinz *et al.*, 2005). Only these force-fields were tested in the present study, therefore. Also, a better description of the hydrated interlayer structure with the *ClayFF* force field can be achieved, according to Ferrage *et al*. (2011), if the Lennard-Jones (LJ) parameters of clay-surface oxygens are increased by ~7%.

The interatomic interaction parameters for EG can be selected from a wide range of different organic force fields. These force fields are usually parameterized to optimize the description of certain specific sets of organic molecules. For example, *CHARMM* was constructed to model proteins (MacKerrel *et al.*, 1998); *AMBER*, to model peptides, proteins, and nucleic acids (Cornell *et al.*, 1995); *OPLS-aa*, for simulations of liquid hydrocarbons (Jorgensen *et al.*, 1996); and *CVFF*, for amino acids, hydrocarbons, and many other organic molecules (Dauber-Osguthorpe *et al.*, 1988). More recent parameterizations which belong to a certain earlier family but were later re-optimized for a larger set of organic molecules include *CHARMM*-related *CGenFF* (general force field for drug-like molecules; Vanommeslaeghe *et al.*, 2009) and *AMBER*-related *GAFF* (general *AMBER* force field; Wang *et al.*, 2004). For the purpose of the present study, the parameterization of a given family that was best optimized for small organic molecules, such as EG, was taken into account.

An even more diverse set of force-field parameterizations for water molecules is available in the literature (*e.g.* Wallqvist and Mountain, 1999; Guillot, 2002; Kalinichev, 2001). In the present study, only the SPC (simple point charge) model of Berendsen *et al.* (1981) is considered because it is known to perform well in combination with *ClayFF*, gives relatively good solution structure for smectite interfaces and interlayers (*e.g.* Heinz *et al.*, 2005; Morrow *et al.*, 2013; Ngouana-Wakou and Kalinichev, 2014; Greathouse *et al.*, 2015), and is also consistent with the *CVFF* and *INTERFACE* parameterizations. The application of different force-field parameterizations for H_2O molecules can, theoretically, affect the simulation results for hydrated clays. The work of Ferrage *et al*. (2011) has shown, however, that using the SPC model is sensible in terms of the agreement of MD simulation results with XRD data.

https://doi.org/10.1346/CCMN.2016.0640411 Published online by Cambridge University Press

Hybrid organo-clay materials are part of a rapidly growing area of molecular simulation studies that requires a reliable coupling of different force-field parameters. Very often *ClayFF* is used together with *CVFF* (*e.g.* Kumar *et al.*, 2006; Liu *et al.*, 2007; Suter and Coveney, 2009; Kalinichev *et al.*, 2010). Examples exist also of the successful use of *ClayFF* in combination with *OPLS-aa* (*e.g.* Schampera *et al.*, 2015), *CHARMM* (*e.g.* Duque-Redondo *et al.*, 2014), and AMBER (*e.g.* Wang *et al.*, 2014; Swadling *et al.*, 2010). The *INTERFACE* force field (Heinz *et al.*, 2013) was developed for use in studies of interactions of organic molecules with minerals, including smectite, together with *CVFF*, *PCFF*, and *COMPASS* organic parameterizations. Other examples of combinations of older clay-mineral force-field parameters with different organic force fields were employed (*e.g.* Tambach *et al.* (2006) used the force field of Skipper *et al.* (1995) together with *OPLS-ua* of Jorgensen and Gao (1986)). Not all of the earlier force-field combinations were tested extensively before they were used in this area of very active current research (much of the work done compared only experimental and simulated basal spacings, *e.g.* Pintore *et al.*, 2001).

At the same time, the structures obtained from molecular simulations using different force-field parameters can be validated by their comparison with available XRD data. This methodology has been used widely for hydrated clay minerals (*e.g.* Ferrage *et al.*, 2011). Even though only the atomic-density distribution of the interlayer species along a direction perpendicular to the layering plane can be considered for turbostratic smectites, it is still a very powerful methodology. Atomic-density distribution was used in the present study to find the optimal set of force-field parameters for organic molecules interacting with smectites.

METHODOLOGY

Smectite samples

Three smectite samples from the collection of the Source Clays Repository of The Clay Minerals Society were studied. These have crystal structures with notably different layer charge and charge localization: low-charge montmorillonite (SWy-1), high-charge montmorillonite (SAz-1), and high-charge beidellite (SbCa-1) (Table 1).

The particle-size fractions were separated to avoid contamination with phases other than smectite. All samples were studied in the Ca^{2+} form prepared by means of dialysis.

The samples were sedimented from aqueous solution onto a glass slide. All slides were glycolated as follows: each air-dried sample with ~50% RH was placed in a closed plastic box (15 cm × 15 cm × 3 cm) with EG solution poured into the bottom of the box. The box with sample was heated at 60ºC for 10 h in an oven.

XRD-pattern registration

To minimize EG loss from the EG-smectite complexes, the XRD patterns for all samples were measured directly after glycolation and in an EG-saturated atmosphere. The XRD data were collected in the range from 2 to 60º2θ using a Thermo ARL XRD system (manufactured in Ecublens, Switzerland), CuKα radiation, and a Peltier-cooled solid-state detector. The tube current and voltage were 45 mA and 35 kV, respectively. The following slit sizes from tube to detector were used: 0.9 mm (0.645º), 1.3º Soller, 1.05 mm; sample, 1.0 mm, 1.3º Soller, 0.3 mm. The step size was 0.05º and the counting time was 20 s per step.

Molecular-dynamics simulations

The simulated structural models of smectites were based on the pyrophyllite crystallographic data (Lee and Guggenheim, 1981), with several isomorphic substitutions introduced at particular atomic sites to mimic the smectite samples studied experimentally. All three structures were built by substituting a relevant number of Al atoms with Mg and Si with Al in the octahedral and tetrahedral sheets of the clay structure, respectively. The Mg/Al ordering in the octahedral sheets was introduced following the work of Ortega-Castro *et al.* (2010), *i.e.* maximizing the distance between Mg atoms. The Al/Si ordering in the tetrahedral sheet was random but obeyed the Löwenstein rule, *i.e.* excluding Al−O−Al linkages. The simulation supercell was 8 × 4 × 2 unit cells in the *a*, *b*, and *c* crystallographic directions, respectively (~41.6 Å × 36.1 Å × *z* Å; the value of *z* varied depending on the amount of EG and H_2O in the interlayer space and the force field used).

The total energy of a molecular model is usually described by a sum of Coulombic (electrostatic) inter-

Table 1. Smectites used in the present study.

Smectite	Tetrahedral charge p.h.u.c.*	Octahedral charge p.h.u.c.	Fe in octahedral sheet p.h.u.c.	Particle-size fraction
SWy-1	0.0	0.28	0.20	<0.1 μm
SAz-1	0.0	0.56	0.26	<2.0 μm
SbCa-1	0.50	0.0	0.09	<1.0 μm

* p.h.u.c.: per half unit cell

https://doi.org/10.1346/CCMN.2016.0640411 Published online by Cambridge University Press

actions, short-range non-electrostatic interactions (sometimes referred to as the van der Waals terms), and bonded (intramolecular) interactions:

$$E_{\text{total}} = E_{\text{Coul}} + E_{\text{VDW}} + E_{\text{Bonded}} \quad (1)$$

The bonded terms are especially important for organic molecules and typically include the bond-stretching, angle-bending energy terms, various torsional terms, *etc*. The electrostatic energy is represented by Coulomb's law:

$$E_{\text{Coul}} = \frac{e^2}{4\pi\varepsilon_o} \sum_{i \neq j} \frac{q_i q_j}{r_{ij}} \quad (2)$$

where r_{ij} is the separation distance between the charged atoms i and j, e is the charge of the electron, ε_o is the dielectric permittivity of vacuum (8.85419×10^{-12} F/m), and the partial charges q_i and q_j are usually derived from quantum mechanics calculations and assigned by the specific force-field model. The van der Waals energy term is usually represented by the conventional LJ (12−6) function, and includes the short-range repulsion associated with the increase in energy as two atoms closely approach each other and the attractive dispersion energy:

$$E_{\text{VDW}} = \sum_{i \neq j} D_{o,ij} \left[\left(\frac{R_{o,ij}}{r_{ij}} \right)^{12} - 2 \left(\frac{R_{o,ij}}{r_{ij}} \right)^{6} \right] \quad (3)$$

$D_{o,ij}$ and $R_{o,ij}$ are empirical parameters specific to a particular force field model. The interaction parameters between the unlike atoms are usually calculated according to the so-called Lorentz-Berthelot mixing rules (*e.g.* Allen and Tildesley, 1987): arithmetic mean for the distance parameter, R_o, and the geometric mean for the energy parameter, D_o:

$$R_{o,ij} = \frac{1}{2}(R_{o,i} + R_o,j) \quad (4)$$

$$D_{o,ij} = \sqrt{D_{o,i} D_{o,j}} \quad (5)$$

The Coulombic and van der Waals interactions are excluded for proximate intramolecular (bonded) interactions (*i.e.* 1−2 and 1−3 atom position exclusions) when large organic molecules are modeled.

In the present case, the interatomic interactions involving smectite structures were described using the *ClayFF* (Cygan *et al.*, 2004) and the *INTERFACE* (Heinz *et al.*, 2005) force fields. *GAFF*, *OPLS-aa*, *CGenFF*, and *CVFF* organic force fields were used for EG, while the SPC model was assumed for water molecules (Berendsen *et al.*, 1981). The *INTERFACE* force field was only coupled with the *CVFF* organic force field because of the consistency of its 1-4-scaling factors (value of 1.0). *CGenFF* assumes no scaling, while *OPLS-aa* uses a scaling factor of 0.5 and *GAFF* uses 0.5 for the non-bonded non-electrostatic part of the interaction and 0.8333 for the electrostatic interactions. *ClayFF* has no restrictions on the organic force field with which it can be coupled, because no 1-4 pairs are present in this parameterization. Additionally, in the original clay-mineral force fields, the LJ parameters for basal oxygens, O_b, were modified as suggested by Ferrage *et al.* (2011) (*ClayFFmod* and *INTERFACEmod*). The LJ parameters of tetrahedral Si and Al atoms were also modified in these models to maintain the same Si−O_b and Al−O_b distances as in the original force fields (see Szczerba *et al.*, 2016 and the 'Supplementary Materials' file deposited at The Clay Minerals Society's website: http://www.clays.org/JOURNAL/JournalDeposits.html, for a more detailed discussion). Ewald summation was applied to calculate the long-range corrections to the Coulombic interactions (*e.g.* Allen and Tildesley, 1987) and the cut-off distance was set at 8.5 Å.

A set of different EG compositions around those of Reynolds (1965), 1.7 EG per half unit cell (p.h.u.c.), was covered by the simulations to obtain the basal spacing closest to that observed experimentally. A constant number of interlayer water molecules, 0.8 H_2O p.h.u.c., was assumed. In addition, for the set of parameters that gave the best results in previous calculations, the EG content was set to vary from 1.4 to 2.0 with a step size of 0.2 p.h.u.c., while the water content also varied between 0.0 and 1.2 H_2O p.h.u.c. with a step size of 0.3 p.h.u.c.

For all the models, structural optimizations (total energy minimizations) were performed first, followed by *NPT*-ensemble MD simulations at 1 bar under evolving temperature using a Langevin dynamics algorithm to control the temperature and a Langevin piston to control the pressure. The time step to integrate the equations of atomic motion was set to 1 fs and the dynamic trajectories of all atoms and system properties were recorded every 1 ps. For the first 0.5 ns the temperature was set to 398 K. Then the temperature dropped to 298 K and the simulation continued for 1 ns. From the last 0.5 ns the equilibrium system properties were recorded for further analysis. To exclude any undesirable displacement of the center of mass of the simulated model, in all simulations one atom of the octahedral sheet was fixed at its initial position, but its interactions with all neighboring atoms were still fully accounted for. All MD simulations were performed using the *LAMMPS* computer program (Plimpton, 1995; http://lammps.sandia.gov).

Parameterization of EG molecules with organic force fields

CGenFF parameters were assigned automatically with the help of the on-line tool (cgenff.paramchem.org) using the *NAMD* convention, which was modified to make it consistent with the *LAMMPS* format. *GAFF* parameterization was performed using the *moltemplate* program (moltemplate.org) with charges assigned automatically using the program *TPACM4* available at

https://doi.org/10.1346/CCMN.2016.0640411 Published online by Cambridge University Press

www.scfbio-iitd.res.in/software/drugdesign/charge.jsp (Mukherjee *et al.*, 2011). *CVFF* parameters were assigned automatically using the program *msi2lmp* provided with the *LAMMPS* program. Partial atomic charges were calculated based on the bond increments from the file containing *CVFF* parameters. *OPLS-aa* parameters were also assigned automatically using the *moltemplate* program. Tcl scripts executed in the *VMD* molecular visualization program (Humphrey *et al.*, 1996) were used to generate all input files for *LAMMPS* simulations.

Calculation of the simulated XRD patterns

For every simulated structure, the atomic density distributions of the interlayer species as well as electron density profiles along the direction perpendicular to the layering were calculated. Then all the distributions were symmetrized with respect to the interlayer center and used as an input for calculation of the XRD patterns using the *Sybilla* code (proprietary software owned by the Chevron Corporation). The values of T_{mean}, d spacing, σ^*, and Δd spacing were optimized automatically. The range of <4.5º2θ was excluded from the optimization because, in this range, the effect of super-crystallites becomes important, which is not taken into account by the code. The amount of Fe in the octahedral sheet was taken directly from Table 1 and was not optimized.

T_{mean} is the average thickness calculated for a lognormal distribution of crystallite thicknesses. A variation of this value affects mainly the broadening of the 00l peaks. The d spacing represents the layer-to-layer distance of smectite structures and affects mainly only the positions of 00l maxima. The σ^* parameter is a standard deviation of the Gaussian orientation function of crystallites (Reynolds, 1986). The Δd spacing describes fluctuations in the layer-to-layer distance. The variations in σ^* and Δd spacing parameters affect the relative XRD intensities by a factor that is quite complex to express analytically, but is known to be a monotonic function of 2θ (Reynolds, 1986; Drits and Tchoubar, 1990). Generally, the largest modification of the relative intensities of 00l reflections is influenced by the structure of interlayer species, which depends on the force fields used.

RESULTS AND DISCUSSION

Comparison of organic force fields for EG

In order to compare the performance of organic force fields in reproducing bulk-liquid EG properties, the density of a box consisting of 230 EG molecules as well as the angular distributions of the torsional O-C-C-O potential energy terms were calculated. The calculated liquid densities are compared with the experimental data in Table 2. The closest agreement is achieved by the *GAFF* parameterization, while all other force fields result in densities noticeably less (*OPLS-aa* and *CGenFF*) or greater (*CVFF*) than the experimental value.

The torsional O−C−C−O angle potential energy distributions were compared to a reference obtained from DFT calculations performed under the B3LYP/DGDZVP level of theory using the *Gaussian* Inc. software package (Frisch *et al.*, 2004). In these calculations, all distances and angles were optimized for a certain O−C−C−O angle. The results (Figure 1) demonstrate that the *CVFF* and *OPLS-aa* force-field parameterizations are the closest to the reference quantum chemical calculation. In the case of *GAFF* parameterization, the *gauche* conformation is predicted to be too stable relative to the *trans* one. On the other hand, the stability of the *trans* conformation is overestimated in the *CGenFF* parameterization. All these differences are important for appropriate modeling of EG conformations in smectite interlayers.

Comparison of intercalate structures with 1.7 EG and 0.8 H_2O p.h.u.c.

The differences observed between the organic force fields, described in the previous section, should have an effect on the simulated interlayer structure and resulting XRD patterns. To study this, the intercalate structure with EG and water content corresponding to that of Reynolds (1965) (1.7 EG and 0.8 H_2O p.h.u.c.) was calculated first. An example for SWy-1 is shown in Figure 2 (the results for two other smectites are provided in the 'Supplementary Materials' file deposited at The Clay Minerals Society's website: http://www.clays.org/JOURNAL/JournalDeposits.html).

The structures obtained using the *INTERFACE* and *INTERFACEmod* force fields are substantially different from those resulting from the application of the *ClayFF* and *ClayFFmod*, *i.e.* oxygen atoms of EG molecules have a much greater tendency to be located closer to the surface than their carbon atoms. In the case of the latter force fields, the positions of the carbon and oxygen atoms closest to the surface do not differ significantly. A similar effect was also observed for water molecules: they are located closer to the clay surface for the *INTERFACE*- than for the *ClayFF*-based models.

Table 2. Comparison of calculated and experimental liquid EG density values

Organic force field	Density at 20ºC (g/cm^3)
OPLS-aa	1.060
GAFF	1.123
CGenFF	1.054
CVFF	1.188
Experimental	1.115[a]

[a] The experimental value of EG density at 20ºC is taken from Dow Chemicals (dow.com/ethyleneglycol/about/properties.htm).

https://doi.org/10.1346/CCMN.2016.0640411 Published online by Cambridge University Press

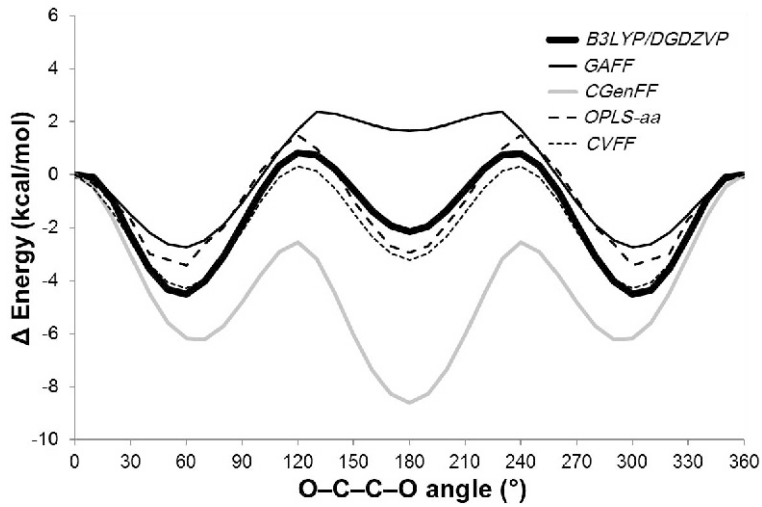

Figure 1. Potential energy scan of the torsional O−C−C−O angle of the EG molecule as reproduced by different organic force fields in comparison with quantum chemical calculations at the B3LYP/DGDZVP level of theory.

Different organic force fields also have significantly different effects on the resulting averaged structures of the intercalate. The effect of different EG liquid density is reflected in the differences in the basal spacings; the lower the density, the greater the basal spacing. No obvious relation exists between the relative stabilities of the *trans-gauche* conformers observed (Figure 1) and the interlayer structures obtained. The positions of carbon atoms are relatively similar for all of the organic force fields tested, while substantial differences were found in the positions of the oxygen atoms of EG. These differences do not affect substantially the electron density profiles calculated, however (Figure 3 and the 'Supplementary Materials' file deposited at The Clay Minerals Society's website: http://www.clays.org/JOURNAL/JournalDeposits.html).

The modification of the LJ parameters for the basal oxygens of smectites leads to a very slight modification of the basal spacing. The modification affects the interlayer structure in such a way, however, that organic and H_2O molecules are located at somewhat greater distances from the clay surface than in the original *ClayFF* models (Figure 2). The same tendency was observed by Ferrage *et al.* (2011). These changes, in turn, affect the calculated electron-density profiles (Figure 3).

Comparison of intercalate structures with 0.8 H_2O p.h.u.c. and basal spacing values close to those measured experimentally

Based on the structure proposed by Reynolds (1965) and on the previous MD simulation studies of EG-smectite structure (Szczerba *et al.*, 2014), the water content was estimated to be ~0.8−1.0 molecules p.h.u.c. This value was, therefore, assumed to be a constant and 0.8 p.h.u.c. was used in the present simulations. The EG content was adjusted to achieve basal-spacing values close to those measured experimentally. This is an obvious approximation due to the fact that the water content in the structure will be related to the actual relative humidity, the time between the sample glycolation and XRD measurement, and the conditions of the XRD profile registration. The water and EG content also depend on the glycolation procedure (Mosser-Ruck *et al.*, 2005). Without this approximation, however, the number or necessary calculations would increase dramatically, but without affecting the main conclusions significantly.

The results of the calculations for SWy-1 are presented in Figure 4 (the results for two other smectites are presented in the 'Supplementary Materials' file deposited at The Clay Minerals Society's website: http://www.clays.org/JOURNAL/JournalDeposits.html). The effect of the variation in the EG content on the structures is significant (in comparison to Figure 2), and the main factors affecting the distribution of atoms in the interlayer space are the organic force field and the clay-mineral force field.

Comparison of the calculated XRD patterns

In order to evaluate and further quantify the differences due to the application of different organic force fields in the molecular modeling studies of organic−smectite interactions, all the distributions calculated above were incorporated into the *Sybilla* code to calculate XRD patterns for the simulated structures. The XRD patterns calculated with optimized values of T_{mean}, d spacing, σ^*, and Δd spacing were then compared with experimental equivalents (Figures 5−7). The results show significant discrepancies in terms of the XRD patterns obtained for different layer charges as well as for different combinations of force fields. Because XRD is only sensitive to the distribution of electrons (the simulated electron density profiles are

https://doi.org/10.1346/CCMN.2016.0640411 Published online by Cambridge University Press

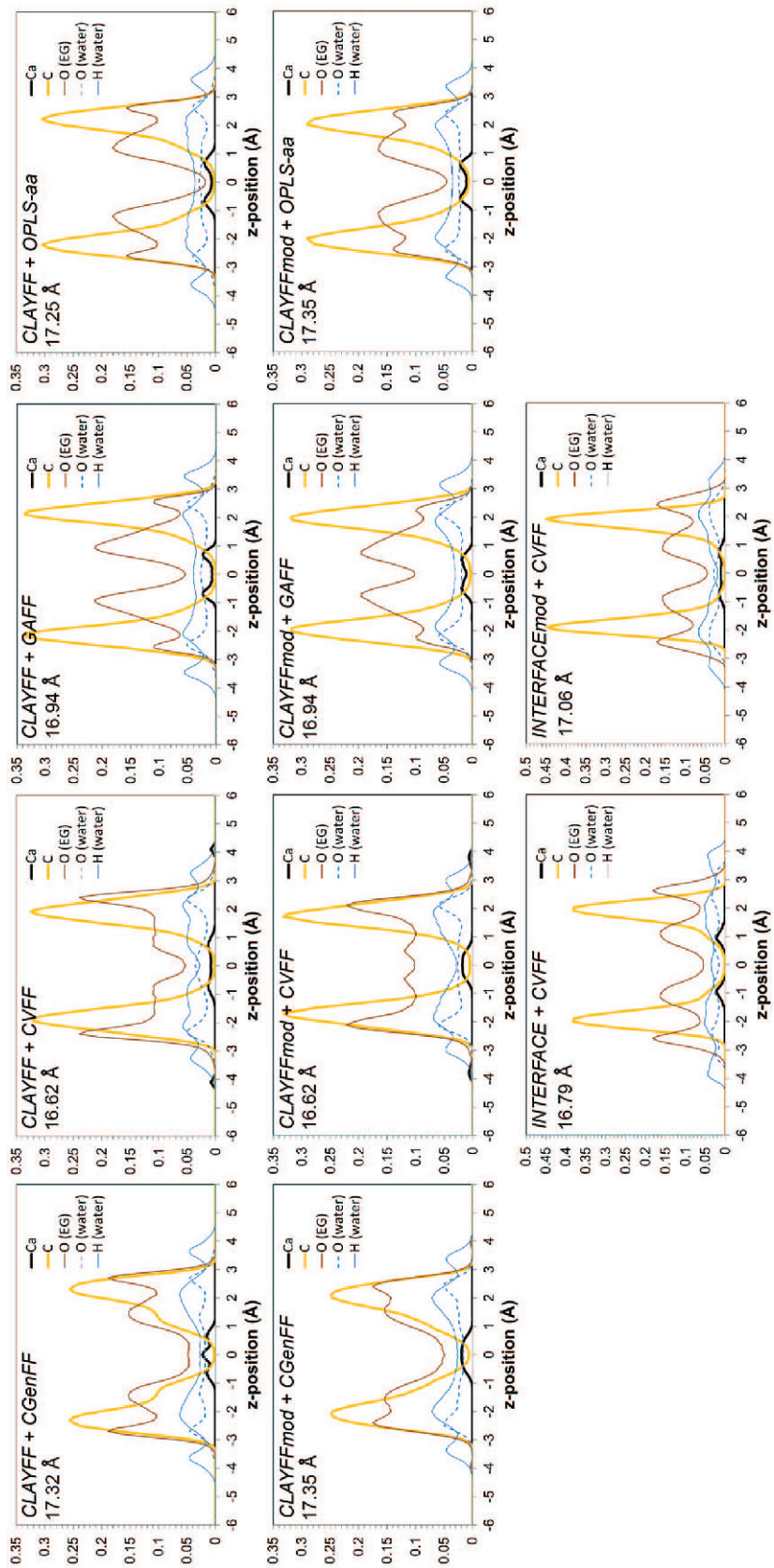

Figure 2. z-density profile distributions for carbon and oxygen of EG, oxygen and hydrogen of water, and Ca^{2+} ions for SWy-1 for 1.7 EG and 0.8 H_2O p.h.u.c. The resulting basal spacings are also shown.

https://doi.org/10.1346/CCMN.2016.0640411 Published online by Cambridge University Press

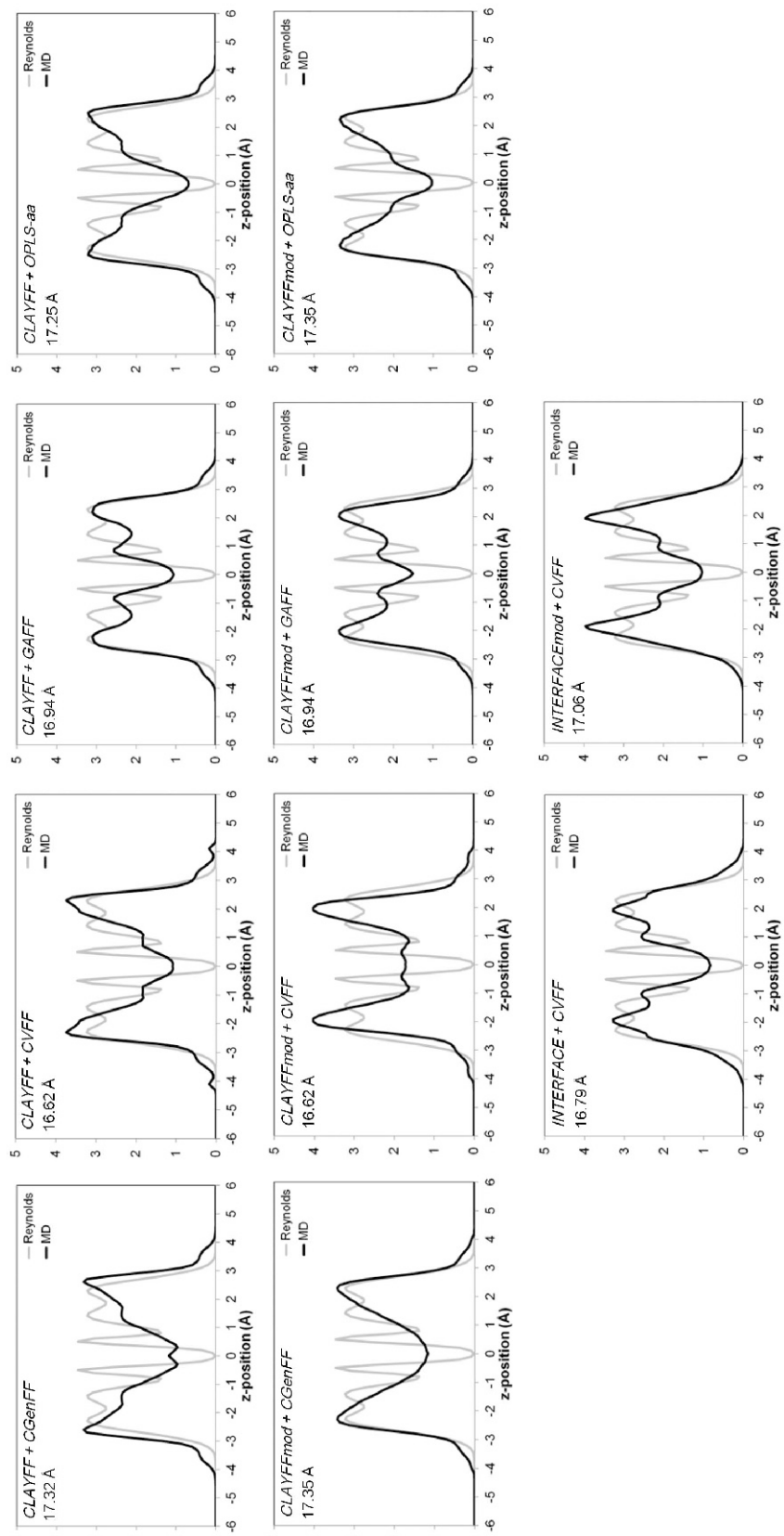

Figure 3. Electron density profiles obtained from MD simulations (black lines) compared to the profiles suggested by Reynolds (1965) (gray lines) for SWy-1 for 1.7 EG and 0.8 H_2O p.h.u.c.

https://doi.org/10.1346/CCMN.2016.0640411 Published online by Cambridge University Press

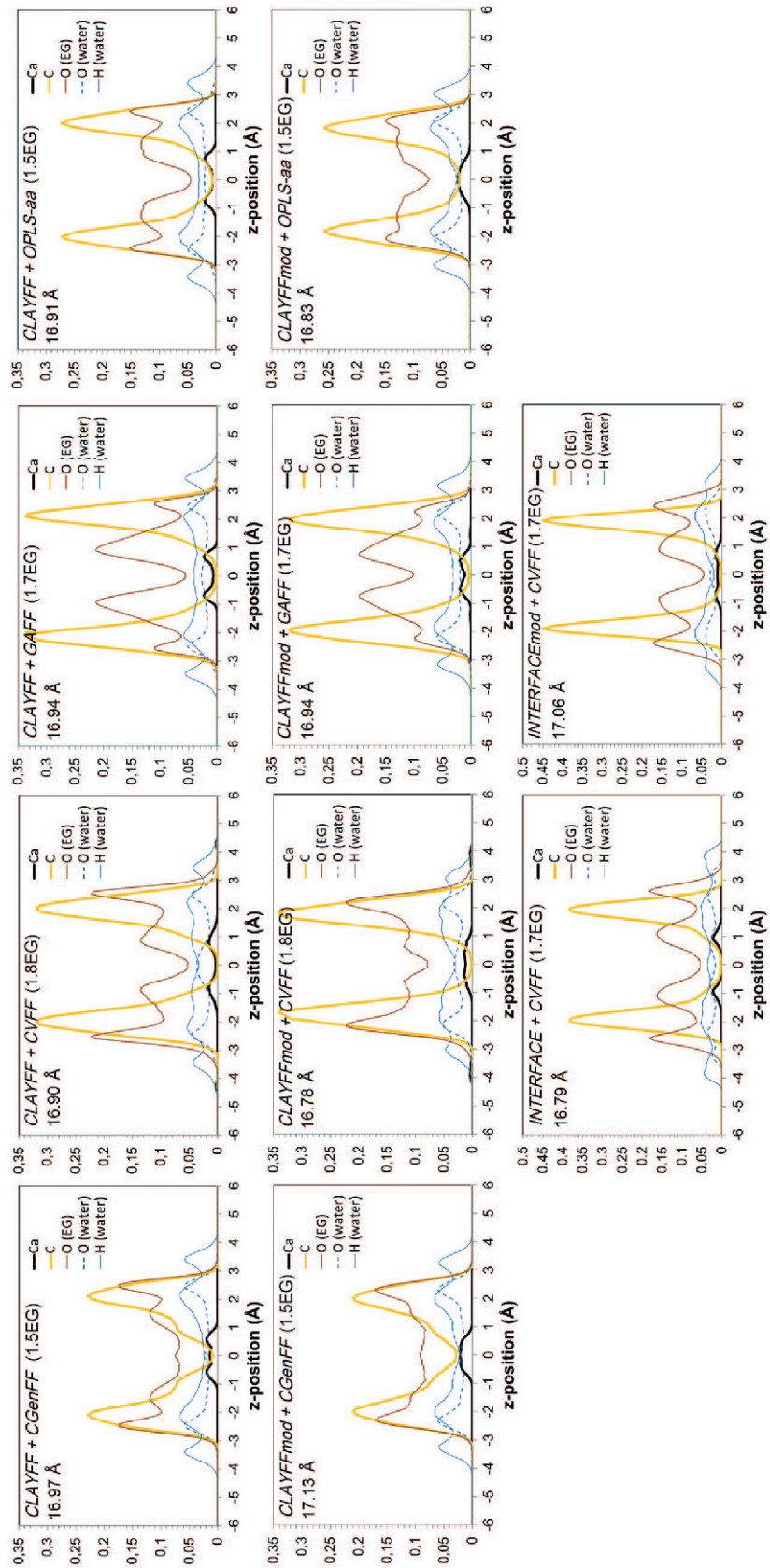

Figure 4. *z*-density profile distributions for carbon and oxygen atoms of EG, oxygen and hydrogen atoms of water, and Ca^{2+} ions for SWy-1 with 0.8 H_2O p.h.u.c. and variable EG content for which the basal spacing is close to 16.92 Å. The resulting basal spacings are also shown.

https://doi.org/10.1346/CCMN.2016.0640411 Published online by Cambridge University Press

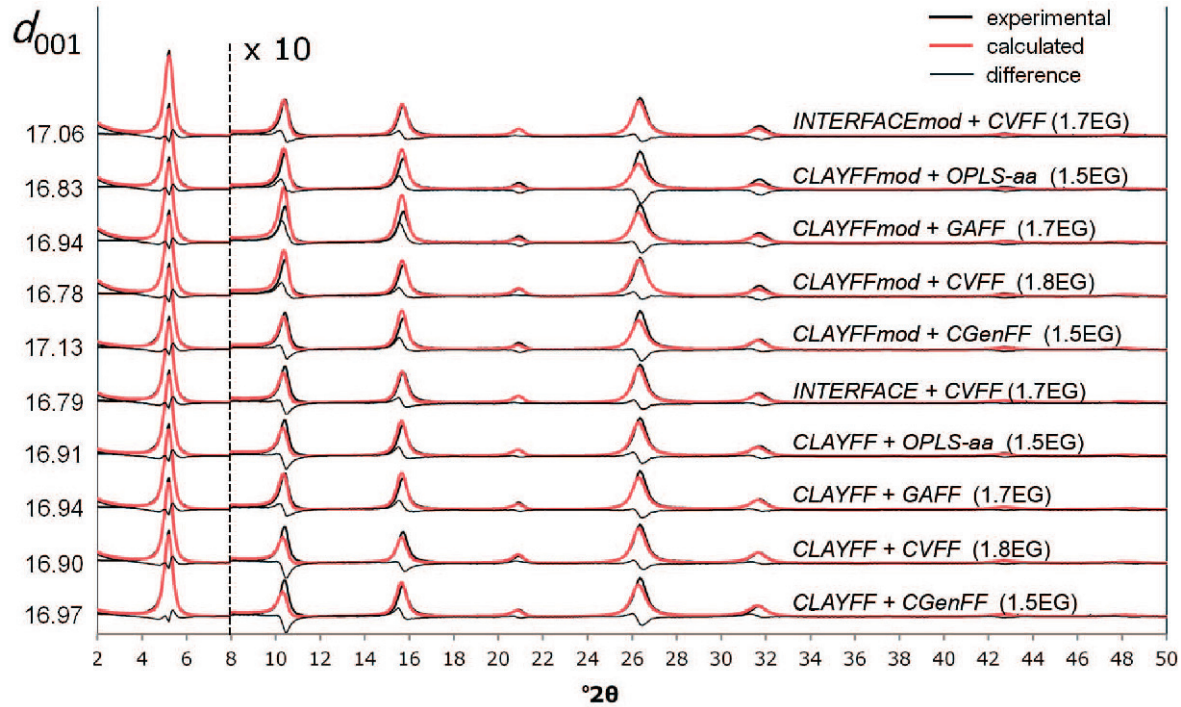

Figure 5. Comparison of XRD patterns of SWy-1 for various force-field combinations.

shown in Figure 3), different electron density profiles may result in different calculated XRD patterns, especially in terms of the distribution of relative 00l intensities.

For low-charge montmorillonite (SWy-1; charge 0.27 p.h.u.c.) the calculated results agree well with experiments for all clay-mineral force fields, and only relatively small differences between the organic force

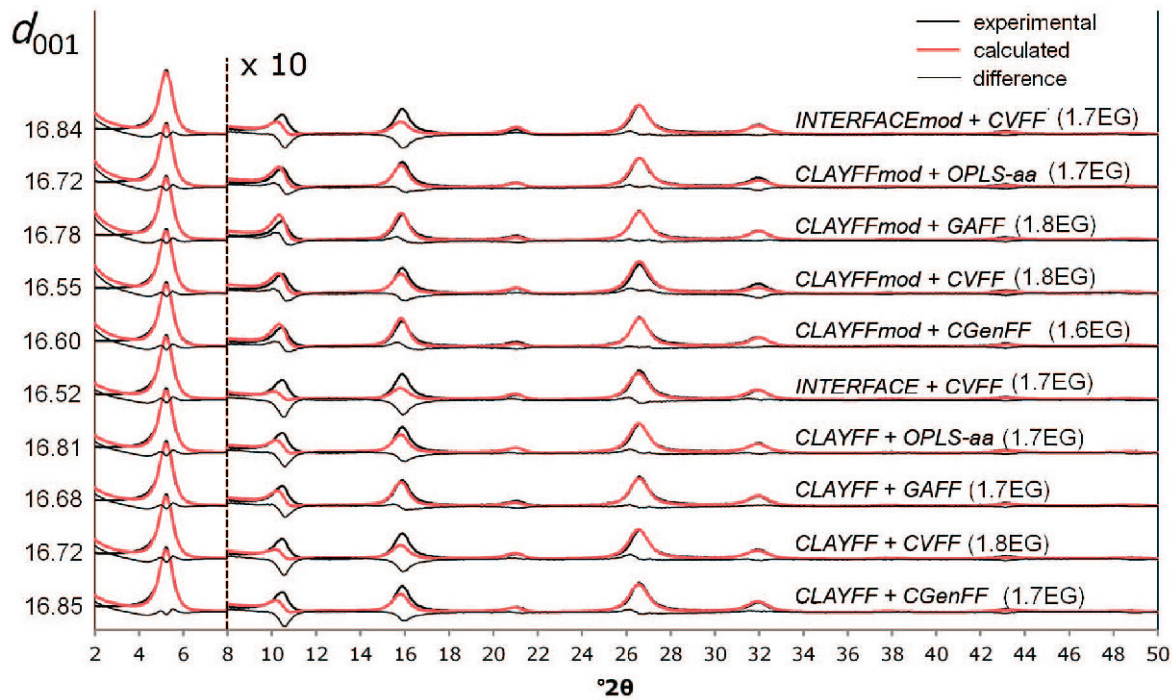

Figure 6. Comparison of XRD patterns of SAz-1 for various force-field combinations.

https://doi.org/10.1346/CCMN.2016.0640411 Published online by Cambridge University Press

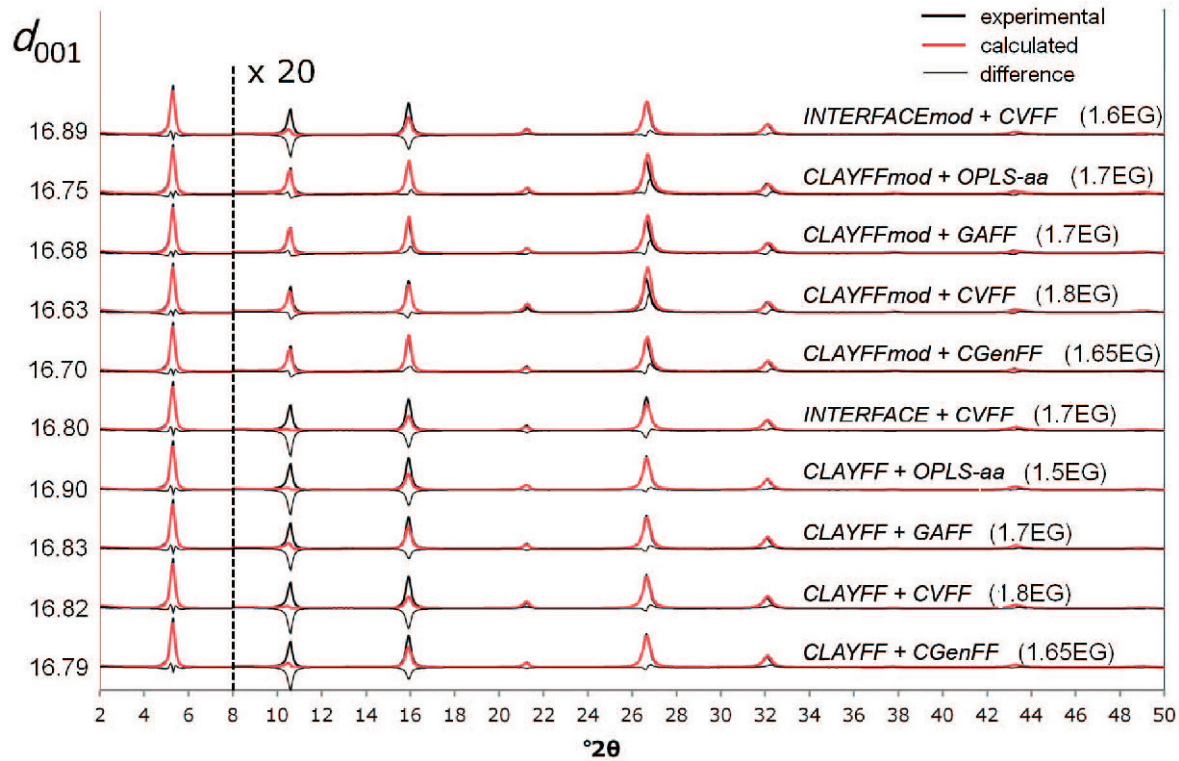

Figure 7. Comparison of XRD patterns of SbCa-1 for various force-field combinations.

fields used are noticeable. The modification of the LJ parameters for the basal oxygens leads to some increase in intensities of the 002 and 003 peaks and to a small decrease in intensities of the 004, 005, and 006 peaks.

For high-charge montmorillonite (SAz-1; charge 0.54 p.h.u.c.) and beidellite (SbCa-1; charge 0.50 p.h.u.c.), the modification of the LJ basal oxygen parameters of the *ClayFF*-based models improved substantially the agreement between the theoretical and experimental XRD patterns for all the organic force fields tested. A substantial correction of the 002 and 003 peak intensities toward those of experimental values was observed. A similar modification applied to the *INTERFACE*-based models led to only relatively small improvement. This indicates that, although *INTERFACE* provides a good structure for low-charge montmorillonites, use of it should probably be modified to describe more accurately the interlayer structure of high-charge smectites.

Among the organic force fields, the least accurate results were obtained when using *CGenFF*. This is probably related to its overestimation of the *trans*-EG molecular conformation and its poor agreement of the EG liquid density with experiment (Figure 1, Table 2). Combined with unmodified *ClayFF*, *GAFF* gives the best results. The resulting XRD pattern was, however, poor for high charge-beidellite in any combination of organic force field with an unmodified clay-mineral set of parameters. The two other sets (*OPLS-aa* and *CVFF*) gave the best results for *ClayFFmod*. The differences observed can be related to the approximations of the organic, clay mineral, and water force fields and to possible uncertainties in the number of EG and water molecules in the interlayer space estimated from experimental data and assumed in the models.

Comparison of the structures with different water and EG contents

Based on the results presented in the previous section, one of the two best sets of force-field combinations (*ClayFFmod* + *CVFF*) was used to study the interlayer structures further and to check if the variation of the assumed EG and water content can improve the calculated XRD patterns. A range of EG compositions was probed systematically between 1.4 and 2.0 p.h.u.c. with a step size of 0.2 p.h.u.c. and with water contents varying between 0.0 and 1.2 p.h.u.c and using a step size of 0.3 p.h.u.c.. The variation in *d* spacing depending on the EG and water content (Figure 8) shows a plateau at ~16.5−17.0 Å with some further variation depending on the layer charge. Based on these plots, several structures were selected (black circles in Figure 8) to calculate average atomic distributions and then to calculate the corresponding XRD patterns for two-layer intercalate structures.

The best of the calculated XRD patterns shows only a small improvement compared to the results shown in Figures 5−7 (Figure 9; all results are presented in the

https://doi.org/10.1346/CCMN.2016.0640411 Published online by Cambridge University Press

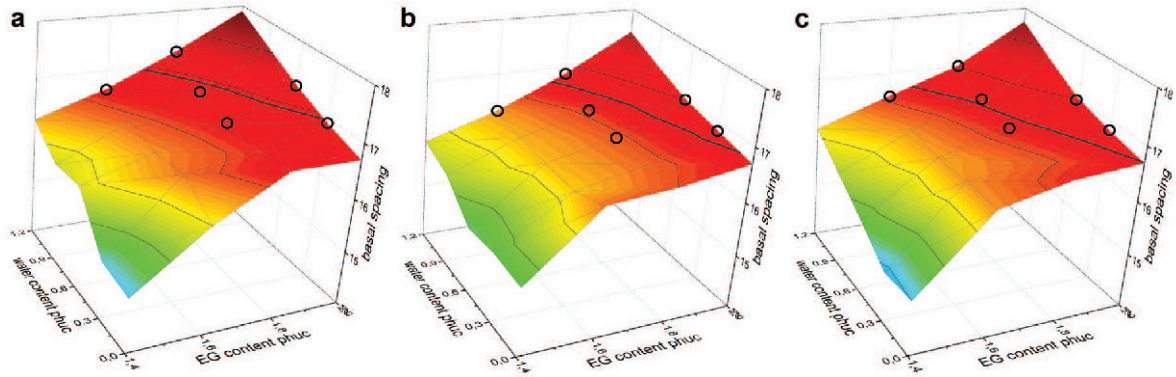

Figure 8. *d*-spacing dependence on the EG and water content for: (a) SWy-1; (b) SAz-1; and (c) SbCa-1 smectites. Small circles mark the structures which were used to calculate the XRD patterns. Thick black lines correspond to experimental basal spacings.

'Supplementary Materials' file deposited at The Clay Minerals Society's website: http://www.clays.org/JOURNAL/JournalDeposits.html). The discrepancy between the simulated and experimental XRD patterns can, therefore, be attributed primarily to the inaccuracy of the force fields used. The most important factor is clearly the selection of the clay-mineral force field; its parameters may require additional improvement.

CONCLUSIONS

The main factor affecting the accuracy of the XRD patterns calculated for EG-water intercalate in smectites is the force field selected to model the clay-mineral substrate. The selection of organic force-field parameters, although also important, has only a secondary effect on the results obtained. The best set of parameters for smectite was found to be *ClayFF* with modified LJ parameters of the basal surface oxygens (*ClayFFmod*). All the organic force fields tested performed relatively well in combination with *ClayFFmod* and the small differences between them depended on the value and location of the smectite charge. Among the organic force fields tested, *GAFF*, *OPLS-aa*, and *CVFF* generally performed relatively well, while the application of *CGenFF* led to the least accurate results.

The *INTERFACE* force field produced relatively good results for low-charge montmorillonite, but it

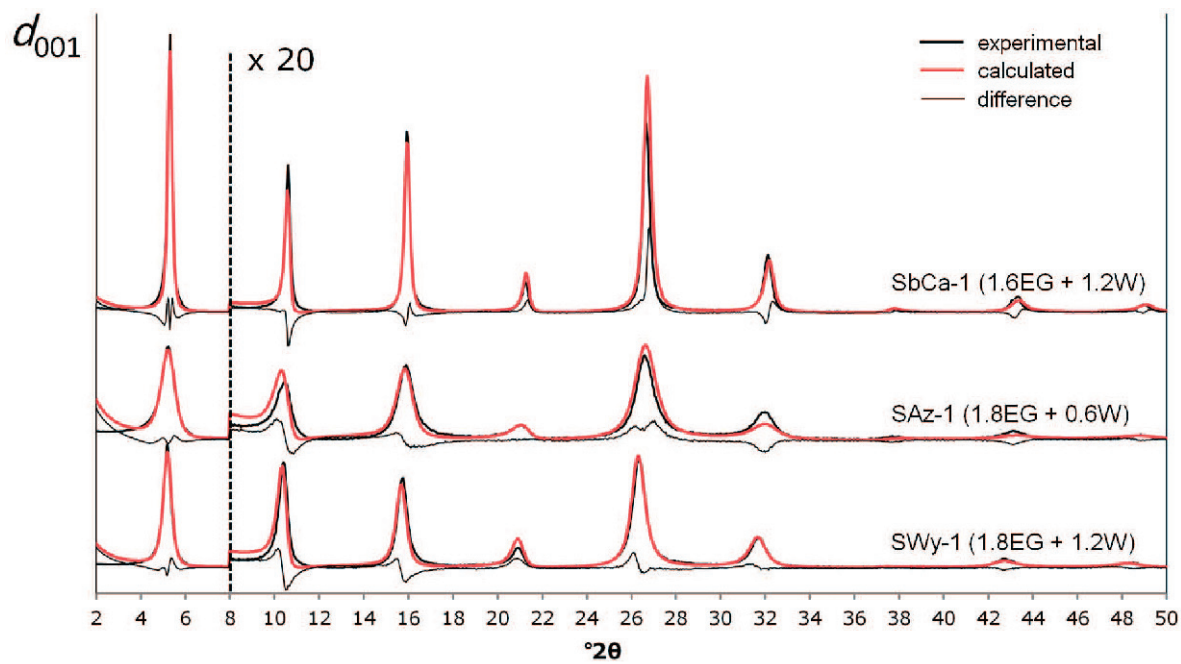

Figure 9. Comparison of XRD patterns for different smectites selected from the compositions in Figure 8 which provide the best agreement between experimental and theoretical diffraction patterns.

https://doi.org/10.1346/CCMN.2016.0640411 Published online by Cambridge University Press

performed less well for high-charge smectites. Unlike *ClayFF*, modifications of the LJ parameters for *INTERFACE* did not help much to improve the resulting XRD patterns simulated. The origin of the discrepancy between the simulated and experimental XRD patterns is apparently in the overestimation of the interlayer atomic populations close to the clay surface.

Further assessment of molecular models could be performed using neutron diffraction. This would help, in particular, to discriminate between models giving relatively similar electron density profiles but contrasting distributions of interlayer hydrogen atoms. Using this approach, the positions of water molecules in the interlayer space of smectite complexes with organic molecules could be determined much more precisely.

ACKNOWLEDGMENTS

The present project was made possible with the financial support of the Polish National Science Centre (grant 2012/05/B/ST10/01948), which provided the Institute of Geological Sciences, PAS, with a high-performance computing server. Computer-time allocations made available within the Distributed European Computing Initiative (project DEC07_NUWCLAY and DEC11 COMPCLAY by the PRACE-2IP receiving funding from the European Community's FP7/2007–2013 under grant agreement RI-283493) and within PLGRID infrastructure are also acknowledged gratefully. AGK was also supported by the industrial chair 'Storage and Disposal of Radioactive Waste' at the Ecole des Mines de Nantes, France, funded by ANDRA, Areva, and EDF.

REFERENCES

Allen, M.P. and Tildesley, D.J. (1987) *Computer Simulation of Liquids*. Oxford University Press, New York, 385 pp.

Berendsen, H.J.C., Postma, J.P.M., van Gunsteren, W.F., and Hermans, J. (1981) Interaction models for water in relation to protein hydration. Pp. 331–342 in: *Intermolecular Forces* (B. Pullman, editor). D. Reidel, Dordrecht, The Netherlands.

Brindley, G.W. (1966) Ethylene glycol and glycerol complexes of smectite and vermiculites. *Clay Minerals*, **6**, 237–259.

Cornell, W.D., Cieplak, P., Bayly, C.I., Gould, I.R., Merz, K.M. Jr., Ferguson, D.M. Spellmeyer, D.C., Fox, T., Caldwell, J.W., and Kollman, P.A. (1995) A second generation force field for the simulation of proteins, nucleic acids and organic molecules. *Journal of the American Chemical Society*, **117**, 5179–5197.

Cygan, R.T., Liang, J.J., and Kalinichev, A.G. (2004) Molecular models of hydroxide, oxyhydroxide, and clay phases and the development of a general force field. *Journal of Physical Chemistry B*, **108**, 1255–1266.

Cygan, R.T., Greathouse, J.A., Heinz, H., and Kalinichev, A.G. (2009) Molecular models and simulation of layered minerals. *Journal of Materials Chemistry*, **19**, 2470–2481.

Dauber-Osguthorpe, P., Roberts, V.A., Osguthorpe, D.J., Wolff, J., Genest, M., and Hagler, A.T. (1988) Structure and energetics of ligand binding to proteins: E. coli dihydrofolate reductase-trimethoprim, a drug-receptor system. *Proteins: Structure, Function and Genetics*, **4**, 31–47.

Drits, V. and Tchoubar, C. (1990) *X-ray Diffraction by Disordered Lamellar Structures. Theory and Applications to Microdivided Silicates and Carbons*, Springer-Verlag, Berlin, Heidelberg.

Duque-Redondo, E., Manzano, H., Epelde-Elezcano, N., Martínez-Martínez, V., and Lopez-Arbeloa, I. (2014) Molecular forces governing shear and tensile failure in clay-dye hybrid materials. *Chemistry of Materials*, **26**, 4338–4345.

Eberl, D.D., Środoń, J., and Northrop, H.R. (1986) Potassium fixation in smectite by wetting and drying. Pp. 296–326 in: *Geochemical Processes at Mineral Surfaces* (J.A. Davis and K.F. Hayes, editors). American Chemical Society Symposium Series, v**323**, Washington, D.C.

Eberl, D.D., Środoń J., Lee M., Nadeau, P.H., and Northrop, H.R. (1987) Sericite from the Silverton caldera, Colorado: Correlation among structure, composition, origin, and particle thickness. *American Mineralogist*, **72**, 914–934.

Ferrage, E., Sakharov, B.A., Michot, L.J., Delville, A., Bauer, A., Lanson, B., Grangeon, S., Frapper, G., Jimenez-Ruiz, M., and Cuello, G.J. (2011) Hydration properties and interlayer organization of water and ions in synthetic Na-smectite with tetrahedral layer charge. Part 2. Toward a precise coupling between molecular simulations and diffraction data. *Journal of Physical Chemistry C*, **115**, 1867–1881.

Frisch, M.J., Trucks, G.W., Schlegel, H.B., Scuseria, G.E., Robb, M.A., Cheeseman, J.R.T., Montgomery, J.A., Vreven, J.T., Kudin, K.N., Burant, J.C., Millam, J.M., Iyengar, S.S., Tomasi, J., Barone, V., Mannucci, B., Cossi, M., Scalmani, G., Rega, N., Petersson, G.A., Nakatsuji, H., Hada, M., Ehara, M., Toyota, K., Fukuda, F., Hasegawa, J., Ishida, M., Nakajima, T., Honda, Y., Kitao, O., Nakai, H., Klene, M., Li, X., Knox, J.E., Hratchian, H.P., Cross, J.B., Bakken, V., Adamo, C., Jramillo, J., Gomperts, R., Stratmann, R.E., Yazyev, O., Austin, A.J., Cammi, R., Pomelli, C., Ochterski, J.W., Ayala, P.Y., Morokuma, K., Voth, G.A., Salvador, P., Dannenberg, J.J., Zakrzewski, V.G., Dapprich, S., Daniels, A.D., Strain, M.C., Frakas, O., Malick, D.K., Rabuck, A.D., Raghavachari, K., Foresman, J.B., Ortiz, J.V., Cui, Q., Baboul, A.G., Clifford, S., Cislowski, J., Stefanov, B.B., Liu, G., Liashenko, A., Piskorz, P., Komaromi, I., Martin, R.L., Fox, D.J., Keith, T., Al-Laham, M.A., Peng, C.Y., Nanayakkara, A., Challacombe, M., Gill, P.M.W., Johnson, B., Chen, W., Wong, M.W., Gonzalez, C., and Pople, J.A. (2004) *Gaussian-94, Revision C.3*. Gaussian, Inc. Pittsburgh Pennsylvania, USA.

Greathouse, J.A., Hart, D.B., Bowers, G.M., Kirkpatrick, R.J., and Cygan, R.T. (2015) Molecular simulation of structure and diffusion at smectite–water interfaces: Using expanded clay interlayers as model nanopores. *Journal of Physical Chemistry C*, **119**, 17126–17136.

Greathouse, J.A., Johnson, K.L., and Greenwell, H.C. (2014) Interaction of natural organic matter with layered minerals: Recent developments in computational methods at the nanoscale. *Minerals*, **4**, 519–540.

Guillot, B. (2002) A reappraisal of what we have learnt during three decades of computer simulations on water. *Journal of Molecular Liquids*, **101**, 219–260.

Guvench, O. and MacKerell A.D. Jr. (2008) Comparison of protein force fields for molecular dynamics simulations. *Methods in Molecular Biology*, **443**, 63–88.

Harward, M.E. and Brindley, G.W. (1965) Swelling properties of synthetic smectite in relation to lattice substitutions. *Clays and Clay Minerals*, **13**, 209–222.

Harward, M.E., Carstea, D.D., and Sayegh, A.H. (1969) Properties of vermiculite and smectites: Expansion and collapse. *Clays and Clay Minerals*, **16**, 437–447.

Heinz, H., Koerner, H., Anderson K.L., Vaia, R.A., and Farmer, B.L. (2005) Force field for mica-type silicates and dynamics of octadecylammonium chains grafted to montmorillonite. *Chemistry of Materials*, **17**, 5658–5669.

Heinz, H., Lin, T.J., Mishra, R.K., and Emami, F.S. (2013) Thermodynamically consistent force fields for the assembly

of inorganic, organic, and biological nanostructures: The INTERFACE force field. *Langmuir*, **29**, 1754–1765.

Heinz, H. and Ramezani-Dakhel, H. (2016) Simulations of inorganic–bioorganic interfaces to discover new materials: insights, comparisons to experiment, challenges, and opportunities. *Chemical Society Reviews*, 45, 412–448.

Hill, J.-R. and Sauer, J. (1995) Molecular mechanics potential for silica and zeolite catalysts based on ab initio calculations. 2. Aluminosilicates. *Journal of Physical Chemistry*, **99**, 9536–9550.

Humphrey, W., Dalke, A., and Schulten, K. (1996) VMD – Visual Molecular Dynamics. *Journal of Molecular Graphics*, **14**, 33–38.

Jorgensen, W.L. and Gao, J. (1986) Monte Carlo simulations of the hydration of ammonium and carboxylate ions. *The Journal of Physical Chemistry*, **90**, 2174–2182.

Jorgensen,W.L., Maxwell, D.S., and Tirado-Rives, J. (1996) Development and testing of the OPLS all-atom force field on conformational energetics and properties of organic liquids. *Journal of the American Chemical Society*, **118**, 11225–11236.

Kalinichev, A.G. (2001) Molecular simulations of liquid and supercritical water: Thermodynamics, structure, and hydrogen bonding. Pp. 83–129 in: *Molecular Modeling Theory: Applications in the Geosciences* (R.T. Cygan and J.D. Kubicki, editors). Reviews in Mineralogy & Geochemistry, **42**, Mineralogical Society of America, Washington D.C.

Kalinichev, A.G., Kumar, P.P., and Kirkpatrick, R.J. (2010) Molecular dynamics computer simulations of the effects of hydrogen bonding on the properties of layered double hydroxides intercalated with organic acids. *Philosophical Magazine*, **90**, 2475–2488.

Kumar, P.P., Kalinichev, A.G., and Kirkpatrick, R.J. (2006) Hydration, swelling, interlayer structure, and hydrogen bonding in organolayered double hydroxides: Insights from molecular dynamics simulation of citrate-intercalated hydrotalcite. *Journal of Physical Chemistry B*, **110**, 3841–3844.

Lee, J.H. and Guggenheim, S. (1981) Single crystal X-ray refinement of pyrophyllite-1Tc. *American Mineralogist*, **66**, 350–357.

Liu, X., Lu, X., Wang, R., Zhou, H., and Xu, S. (2007) Interlayer structure and dynamics of alkylammonium-intercalated smectites with and without water: A molecular dynamics study. *Clays and Clay Minerals*, **55**, 554–564.

MacKerell, Jr. A.D., Bashford, D., Bellott, M., Dunbrack, R.L., Evanseck, J.D., Field, M.J., Fischer, S. Gao, J. , Guo, H., Ha, S., Joseph-McCarthy, D., Kuchnir, L., Kuczera, K., Lau, F.T.K., Mattos, C., Michnick, S., Ngo, T., Nguyen, D.T., Prodhom, B., Reiher III, W.E., Roux, B., Schlenkrich, M., Smith, J.C., Stote, R., Straub, J., Watanabe, M., Wiórkiewicz-Kuczera, J., Yin, D., and Karplus, M. (1998) All-atom empirical potential for molecular modeling and dynamics studies of proteins. *Journal of Physical Chemistry B*, **102**, 3586–3616.

Manevitch, O.L. and Rutledge, G.C. (2004) Elastic properties of a single lamella of montmorillonite by molecular dynamics simulation. *Journal of Physical Chemistry B*, **108**, 1428–1435.

Morrow, C.P., Yazaydin, A.Ö., Krishnan, M., Bowers, G.M., Kalinichev, A.G., and Kirkpatrick, R.J. (2013) Structure, energetics, and dynamics of smectite clay interlayer hydration: Molecular dynamics and metadynamics investigation of Na-hectorite. *Journal of Physical Chemistry C*, **117**, 5172–5187.

Mosser-Ruck, R., Devineau, K., Charpentier, D., and Cathelineau, M. (2005) Effects of ethylene glycol saturation protocols on XRD patterns: A critical review and discussion. *Clays and Clay Minerals*, **53**, 631–638.

Mukherjee, G., Patra, N., Barua, P., and Jayaram, B. (2011) A fast empirical GAFF compatible partial atomic charge assignment scheme for modeling interactions of small molecules with biomolecular targets (TPACM4). *Journal of Computational Chemistry*, **32**, 893–907.

Ngouana Wakou, B.F. and Kalinichev, A.G. (2014) Structural arrangements of isomorphic substitutions in smectites: Molecular simulation of the swelling properties, interlayer structure, and dynamics of hydrated Cs-montmorillonite revisited with new clay models. *Journal of Physical Chemistry C*, **118**, 12758–12773.

Ortega-Castro, J., Hernández-Haro, N., Dove, M.T., Hernández-Laguna, A., and Saínz-Diaz, C.I. (2010) Density functional theory and Monte Carlo study of octahedral cation ordering of Al/Fe/Mg cations in dioctahedral 2:1 phyllosilicates. *American Mineralogist*, **95**, 209–220.

Pintore, M., Deiana, S., Demontis, P., Manunza, B., Suffritti, G.B., and Gessa, C. (2001) Simulations of interlayer methanol in Ca-and Na-saturated montmorillonites using molecular dynamics. *Clays and Clay Minerals*, **49**, 255–262.

Plimpton, S. (1995) Fast parallel algorithms for short-range molecular dynamics. *Journal of Computational Physics*, **117**, 1–19.

Reynolds, R.C. (1965) An X-ray study of an ethylene glycol-montmorillonite complex. *American Mineralogist*, **50**, 990–1001.

Reynolds, R.C. (1986) The Lorentz-polarization factor and preferred orientation in oriented clay aggregates. *Clays and Clay Minerals*, **34**, 359.

Sato, T., Watanabe, T., and Otsuka, R. (1992) Effects of layer charge, charge location, and energy change on expansion properties of dioctahedral smectites. *Clays and Clay Minerals*, **40**, 103–113.

Sato, H., Yamagishi, A., and Kawamura, K. (2001) Molecular simulation for flexibility of a single clay layer. *Journal of Physical Chemistry B*, **105**, 7990–7997.

Schampera, B., Solc, R., Woche, S.K., Mikutta, R., Dultz, S., Guggenberger, G., and Tunega, D. (2015) Surface structure of organoclays as examined by X-ray photoelectron spectroscopy and molecular dynamics simulations. *Clay Minerals*, **50**, 353–367.

Skipper, N.T., Refson, K., and McConnell, J.D.C. (1991) Computer simulation of interlayer water in 2:1 clays. *Journal of Chemical Physics*, **94**, 7434–7445.

Skipper, N.T., Chang, F.R.C., and Sposito, G. (1995) Monte Carlo simulation of interlayer molecular structure in swelling clay minerals. I: Methodology. *Clays and Clay Minerals*, **43**, 285–293.

Smith, D.E. (1998) Molecular computer simulations of the swelling properties and interlayer structure of cesium montmorillonite. *Langmuir*, **14**, 5959–5967.

Svensson, P.D. and Hansen, S. (2010) Intercalation of smectite with liquid ethylene glycol ù Resolved in time and space by synchrotron X-ray diffraction. *Applied Clay Science*, **48**, 358–367.

Suter, J.L. and Coveney, P.V. (2009) Computer simulation study of the materials properties of intercalated and exfoliated poly (ethylene) glycol clay nanocomposites. *Soft Matter*, **5**, 2239–2251.

Suter, J.L., Coveney, P.V., Anderson, R.L., Greenwell, H.C., and Cliffe, S. (2011) Rule based design of clay-swelling inhibitors. *Energy & Environmental Science*, **4**, 4572–4586.

Suter, J.L., Groen, D., and Coveney, P.V. (2015) Chemically specific multiscale modeling of clay-polymer nanocomposites reveals intercalation dynamics, tactoid self-assembly and emergent materials properties. *Advanced Materials*, **27**, 966–984.

Swadling, J.B., Coveney, P.V., and Greenwell, H.C. (2010)

Clay minerals mediate folding and regioselective interactions of RNA: a large-scale atomistic simulation study. *Journal of the American Chemical Society*, **132**, 13750–13764.

Szczerba, M., Kłapyta, Z., and Kalinichev, A.G. (2014) Ethylene glycol intercalation in smectites. Molecular dynamics simulation studies. *Applied Clay Science*, **91–92**, 87–97.

Szczerba, M., Kuligiewicz, A., Derkowski, A., Gionis, V., Chryssikos, G.D., and Kalinichev, A.G. (2016) Structure and dynamics of water–smectite interfaces: Hydrogen bonding and the origin of the sharp $O\text{-}D_w/O\text{-}H_w$ infrared band from molecular simulations. *Clays and Clay Minerals*, **64**, 452–471.

Środoń, J. (1980) Precise identification of illite/smectite interstratification by X-ray powder diffraction. *Clay and Clay Minerals*, **28**, 401–411.

Tambach, T.J., Bolhuis, P.G., Hensen, E.J., and Smit, B. (2006) Hysteresis in clay swelling induced by hydrogen bonding: accurate prediction of swelling states. *Langmuir*, **22**, 1223–1234.

Teppen, B.J., Rasmussen, K.R., Bertsch, P.M., Miller, D.M., and Schafer, L. (1997) Molecular dynamics modeling of clay minerals. 1. Gibbsite, kaolinite, pyrophillite, and beidellite. *The Journal of Physical Chemistry B*, **101**, 1579–1587.

Vanommeslaeghe, K., Hatcher, E., Acharya, C., Kundu, S., Zhong, S., Shim, J., Darian, E., Guvench, O., Lopes, P., Vorobyov, I., and Mackerell, A.D. Jr. (2009) CHARMM general force field: A force field for drug-like molecules compatible with the CHARMM all-atom additive biological force fields. *Journal of Computational Chemistry*, **31**, 671–90.

Wallqvist, A. and Mountain, R.D. (1999) Molecular models of water: Derivation and description. Pp. 183–247: *Reviews in Computational Chemistry* (D.B.B. Kenny and B. Lipkowitz, editors), vol. **13**. John Wiley & Sons, Inc., New York.

Wang, J., Wolf, R.M., Caldwell, J.W., Kollman, P.A., and Case, D.A. (2004) Development and testing of a general amber force field. *Journal of Computational Chemistry*, **25**, 1157–74.

Wang, Y., Wohlert, J., Bergenstrahle-Wohlert, M., Kochumalayil, J.J., Berglund, L.A., Tu, Y., and Ågren, H. (2014) Molecular adhesion at clay nanocomposite interfaces depends on counterion hydration–molecular dynamics simulation of montmorillonite/xyloglucan. *Biomacromolecules*, **16**, 257–265.

Zeng, Q.H., Yu, A.B., Lu, G.Q., and Standish, R.K. (2003) Molecular dynamics simulation of organic-inorganic nanocomposites: Layering behavior and interlayer structure of organoclays. *Chemistry of Materials*, **15**, 4732–4738.

(*Received 29 February 2016; revised 31 October 2016; Ms. 1093; AE: Xiandong Liu*)